

1 **Assessing flooding impact to riverine bridges: an integrated analysis**

2 Maria Pregnolato^{1*}, Andrew O. Winter², Dakota Mascarenas², Andrew D. Sen³, Paul Bates⁴, Michael R.
3 Motley²

4 ¹Dep. of Civil Engineering, University of Bristol, Bristol, BS8 1TR, UK

5 ²Dep. of Civil and Environmental Engineering, University of Washington, Seattle, 98103, USA

6 ³Dep. of Civil, Construction and Environmental Engineering, Marquette University, Milwaukee, 53233, USA

7 ⁴School of Geographical Sciences, University of Bristol, Bristol, BS8 1RL, UK

8 *Correspondence to: Maria Pregnolato (maria.pregnolato@bristol.ac.uk)

9 **Abstract.** Flood events are the most frequent cause of damage to infrastructure compared to any other natural hazard, and
10 global changes (climate, socio-economic, technological) are likely to increase this damage. Transportation infrastructure
11 systems are responsible for moving people, goods, and services, and ensuring connection within and among urban areas. A
12 failed link in this system can impact the community by threatening evacuation capability, recovery operations and the overall
13 economy. Bridges are critical links in the wider urban system since they are associated with little redundancy and a high
14 (re)construction cost. Riverine bridges are particularly prone to failure during flood events; in fact, the risks to bridges from
15 high river flows and bank erosion have been recognized as crucial at global level. The interaction among flow, structure and
16 network is complex, and not fully understood. This study aims to establish a rigorous, multiphysics modelling approach for
17 the hydrodynamic forces impacting inundated bridges, and the subsequent structural response, while understanding of the
18 consequences of such impact on the surrounding network. Objectives of this study are to model hydrodynamic forces as
19 demand on the bridge structure, to advance a performance evaluation of the structure under the modelled loading, and to assess
20 the overall impact at systemic level. The flood-prone city of Carlisle (UK) is used as case study and a proof of concept.
21 Implications of the hydrodynamic impact on the performance and functionality of the surrounding transport network are
22 discussed. This research will help to fill the gap between current guidance for design and assessment of bridges within the
23 overall transport system.

24 **1 Introduction**

25 Bridges are crucial elements of the transport network given their high construction costs and the lack of alternatives routes.
26 Man-made and natural events are a threat to bridge safety and network serviceability (Yang and Frangopol, 2020). Bridges act
27 as bottlenecks for surrounding roads, and thus any service disruption can knock-out communities' access and connections,
28 impair emergency planning and evacuation routes, as well as impact economies and businesses.

29 Some disruptive events are growing in frequency and severity. In particular, the impacts of flooding have been exacerbated in
30 recent years by urbanisation (e.g. increase of impermeable surfaces), inappropriate land use in flood-prone areas and climate
31 change. Rainfall events that lead to flooding are becoming more frequent and intense (Solomon et al., 2007), triggering bridge
32 incidents and failures all over the world (Cumbria, UK, 2009; Drake, Colorado, 2013; Texas, 2018; Greece, 2020). As recent
33 examples, Grinton Bridge in Yorkshire (North-West UK) and Keritis Bridge in Crete (Greece) were both washed away by
34 floodwaters in 2019.

35 Riverine bridges are intrinsically vulnerable to flooding, as they are located in the area of the riverbed. Flood and scour
36 represent one of the most frequent causes of bridge failures (Hunt, 2009; Wardhana and Hadipriono, 2003; Khan, 2015;
37 Ahamed et al., 2020). Although, scour is recognized as the biggest threat, available scour-related literature is much more
38 robust, and hydrodynamic forces could be as critical for bridge piers on bedrock (where scour is unlikely), and for the decks
39 of all flooded bridges (Kim et al., 2017; Oudenbroek et al., 2018). In terms of consequences, natural hazards can damage
40 bridges structurally (thus causing direct physical damages), but these events can also result in functional failures that cause

41 travel time delays and rerouting that lead to indirect losses. Any bridge failure, whether structural or functional, has the
42 potential to impose heavy consequences to owners or responsible authorities, as well as dire expenses. Therefore,
43 understanding the potential impact of flooding to bridges is a compelling need of communities in areas of high flood risk.
44 Currently, a limited number of studies investigated the consequences of extreme flooding to bridges and the surrounding
45 network (Yang and Frangopol, 2020). Practical application and case studies of real bridges tend to be focused on other natural
46 hazards (e.g. earthquakes: Kilanitis and Sextos, 2019, Ertugay et al., 2016; Zhou et al., 2010). This study aims to establish a
47 rigorous, multiphysics modelling approach for assessing hydrodynamic forces on inundated bridges, subsequent structural
48 response, and consequences of such impact on the surrounding network. Objectives of this study are to model hydrodynamic
49 forces as demand on the bridge structure, to advance a performance evaluation of the structure under the modelled loading,
50 and to assess the overall impact at systemic level. Implications of the hydrodynamic impact on the performance and
51 functionality of the surrounding transport network are discussed. This research will help to fill the gap between current
52 guidance for design and assessment of bridges within the overall transport system.

53 **1.1 Background**

54 Transport networks are formed by multiple links (i.e. roads), and their performance relies on a number of parameters, such as
55 availability of alternative routes (redundancy), road capacity, or traffic demand, among others. A bridge failure often means a
56 critical link been taken out of service. Bridges are usually costly assets to be repaired, have little redundancy and are likely to
57 be crossed by a high number of users, especially if belonging to strategic road networks (e.g. highways). Therefore, bridge
58 closure or failure can impact the overall performance of the road network and the failure consequences have to be investigated
59 from a system-perspective (Yang and Frangopol, 2020). The assessment of the systemic impact is a complex and multi-
60 disciplinary problem, at the interface of hydrology, fluid dynamics, structural analysis and transport modelling.

61 Scour damage is a significant concern for many bridge structures and has been extensively studied (e.g. Pregolato et al.,
62 2021a; Wang et al., 2017; Hung and Yau, 2017; AASHTO, 2002); the more common methods include using the HEC-18
63 (Arneson et al., 2012) or CIRIA scour equations (Kirby et al., 2015; HE, 2012). however, it is not the main focus of this paper
64

65 On the contrary, literature about modeling the hydrodynamic forces of the fluid on bridges due to riverine floods is limited,
66 especially concerning fragility models or reliability analysis (Pregolato, 2019; Gidaris et al., 2017). Existing research
67 investigated tsunami impact to bridges (e.g. Motley and al., 2016; Lomonaco et al., 2018; Qin et al., 2018; Winter et al., 2017),
68 where Computational Fluid Dynamics (CFD) techniques are used to compute hydrodynamic forces on bridges and
69 components. Also, Kerenyi et al. (2009) applied CFD to compute hydrodynamic forces on inundated bridge decks, however
70 the analysis was limited to the evaluation of drag and lift forces, without investigating impact and consequences. Multi-hazard
71 studies have investigated the interaction and implication of multiple hazards acting on a single structure (Gidaris et al., 2017;
72 Carey et al., 2019), especially between earthquake and tsunami. Other studies (Mondoro and Frangopol, 2018; Liu et al., 2018;
73 Yilmaz et al., 2016) that tackled flood impact to bridges generally expressed the hazard through flood hazard curves, generated
74 via flood-frequency analysis; however, a detailed hydraulic analysis was beyond the scope of their work. While tsunami
75 loading of bridges will often result in much higher forces than riverine flows, the prevalence of riverine flooding relative to
76 tsunami events necessitate further study and could have a far-reaching effect.

77 **1.2 Motivation and aim**

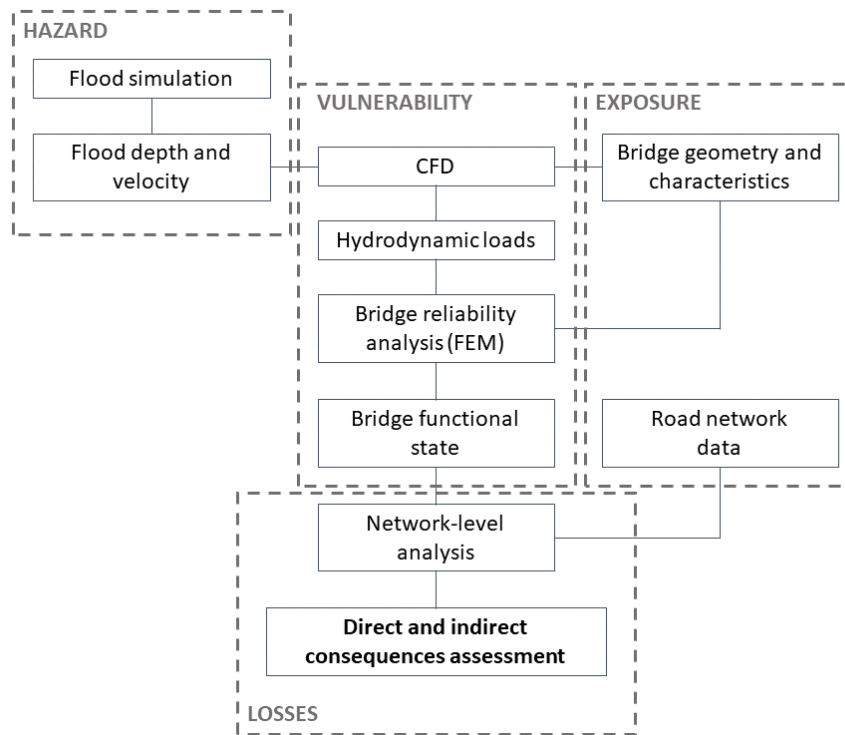
78 To the authors' knowledge, no study has comprehensively investigated the impact of high-river flows on bridges accounting
79 for the complexity of the hydrodynamic forces to which the bridge is subjected and the associated structural and functional
80 response. Moreover, the impact of the reduced service on a bridge on the surrounding network is rarely addressed in the
81 literature. Given this limited availability of models, this paper aims at establishing a multilevel modeling framework to address

82 these issues in one combined approach. This aim is achieved by developing an integrated framework to assess the flooding
83 impact on riverine bridges from the structural- to the network-level (Pregolato et al., 2021b) and applying it to a real case
84 study in the UK. This research tackles varying flow conditions (velocity and depth) to understand the structural response across
85 given simulated flooding conditions. This work is novel since it represents a first attempt to couple CFD analysis with both
86 Finite Element (FE) and network analysis for bridges subjected to flooding, in an effort to capture both the cause and effect of
87 flooding. It is expected that this approach will be useful for understanding structural damage and functional loss for a range of
88 bridges, and ultimately to assess risk for any coastal or riverine structure where large-scale water inundation is expected.

89 **2 Method**

90 This paper adopts a risk-based framework to assess the impact of high river flows to bridges and surrounding roads (Figure 1).
91 The framework proposes a comprehensive method that encompasses the traditional four risk modules (hazard, exposure,
92 vulnerability and consequences; Grossi and Kunreuther, 2005) and includes hydrodynamic force modelling, bridge
93 susceptibility to the hazard, performance evaluation and network-level impact assessment. This study adopts specific
94 models/software, but the precise chosen sub-models are not critical. In fact, all models/software are interchangeable, and it is
95 reasonable to expect that the presented approach would be appropriate for software packages that ensure similar configuration.
96 The first step is to determine the intensity measures of flooding in terms of flow depth and velocity (see Section 2.1). For
97 modelling fluvial flooding, most 2D hydrodynamic models can simulate flood depths and flow velocity, e.g. *LISFLOOD-FP*
98 (<https://bit.ly/3lstd4j>) or *TELEMAC* (<http://www.opentelemac.org/>). Bridge information, such as geometry and design, can be
99 retrieved through publicly available databases (e.g. the US National Bridge Inventory) or by coordination with local
100 infrastructure managers and authorities; such information includes (but is not limited to) bridge dimensions, number of piers,
101 material, design principle, foundation type. Unsurprisingly, the availability and accuracy of data vary from bridge to bridge
102 and can influence the modelling outputs.

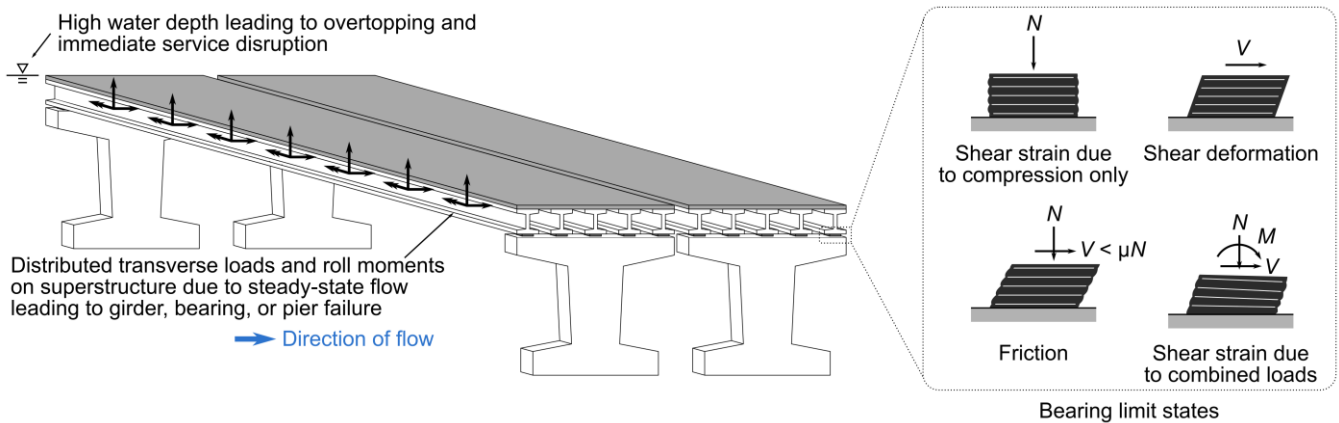
103 The second step consists of modelling the interaction between the water and the bridge, as well as the subsequent flood-induced
104 loads. A simplified vulnerability and criticality assessment (Johnson and Whittington, 2011) include the evaluation of the
105 local flow conditions and corresponding hydrodynamic forces that represent the load on the bridge structure using
106 Computational Fluid Dynamics (CFD) techniques. Here, the C++ toolbox *OpenFOAM* is the adopted software, being open-
107 source and particularly versatile for the development of customized numerical solvers (<https://www.openfoam.org/>).



108

109 **Figure 1: The proposed risk-based methodological flowchart to integrate modelling of hydrodynamic forces, performance and**
 110 **network-level analysis. Acronyms: CFD - Computational Fluid Dynamics; FEM – Finite Element Model.**

111 The third step is to determine the response of the bridge subjected to flood through an advanced structural analysis approach
 112 such as Finite Element (FE) analysis. There are many available FE models, such as Abaqus FEA (www.3ds.com), ANSYS
 113 (<https://www.ansys.com/en-gb>), SAP2000 (<https://www.csiamerica.com/products/sap2000>) or the *OpenSees* software
 114 framework (McKenna et al., 2010). Mondoro and Frangopol (2018) described salient limit states for bridges subjected to
 115 hydraulic loads, and the subset studied in this paper (shown in Figure 2) includes yielding of the girders or piers, unseating or
 116 uplift of the girders, failure of the bearings, and excessive global displacement of the superstructure at which transient fluid-
 117 structure interaction is important (i.e., the CFD modeling approach is limited).



118

119 **Figure 2: Bridge failure states investigated due to flood loading.**

120 The general limit-states philosophy considers that specifications should satisfy “specified limit states to achieve the objectives
 121 of constructability, safety and serviceability” (AASHTO, 2017). In this work, the failure of a bridge is seen as twofold: (i)
 122 structural (also strength limit state), when the bridge deck, piers or foundation reach the ultimate limit state or permanent
 123 deformations; (ii) functional (also service limit state), when the bridge cannot perform its service as usual. A structural failure
 124 directly leads to a functional failure, e.g. the bridge collapses; preventive closure could also take place when bridge conditions
 125 are considered unsafe. Nevertheless, a bridge could be unserviceable but still structurally sound, e.g. when floodwater or debris

126 cover the deck. Hydraulic pressures (drag, lift and overturning moment) are assessed for potentially dislodging the deck from
127 piers, when submerged or partially sub-merged, and overtopping of the deck is evaluated qualitatively from the CFD model.
128 Though these limit states have significantly different long-term consequences, both result in potential functional failure. The
129 importance of long-term effects should be defined based on local transportation needs.
130 The last step is to assess consequences, by including the impact of the bridge failure on the wider transport network. Transport
131 models such as *ESRI™ ArcGIS Network Analyst* (<https://bit.ly/2GPMknl>), *SUMO* (<http://sumo.sourceforge.net/>) or *MatSIM*
132 (<https://www.matsim.org/>) are suitable for computing routing and delays associated with a disrupted network link (such as a
133 closed bridge). Road network data are publicly available from sources such as Digimap® (<https://digimap.edina.ac.uk/>), which
134 provides Ordnance Survey road maps. These contain topographic information of roads including name, location, length,
135 capacity and type. After configuring the transportation network model with the collected data, routing and accessibility can be
136 investigated using network-based spatial analysis and transport appraisal techniques (Arrighi et al., 2020; Pregnotato et al.,
137 2016). This impact analysis links the structural damage of a bridge due to flooding with the reduced performance of the local
138 road network the bridge serves for, approximating the wider consequences.

139 **2.1 Fluvial flooding simulation**

140 Ideally, boundary conditions should be provided by gauging stations; however, no river gauges are present near the bridge of
141 interest, as is often the case in practical scenarios. This study adopted the 2D hydrodynamic model *LISFLOOD-FP*, which
142 allows to simulate flood depths and flow velocity to set up CFD boundary conditions for a flood scenario and from available
143 gauge data.

144 *LISFLOOD-FP* is a two-dimensional, spatially distributed, grid-based hydrodynamic model for simulating channel and
145 floodplain flows (Neal et al., 2009). The model dynamically simulates flood propagation in each grid cell at each time step, on
146 the basis of the local inertial formulation of the shallow water equations and an explicit finite difference method. Numerically,
147 this process involves calculating the momentum equation (the flow between cells given the mass in each cell) and the continuity
148 equation (the change in mass in each cell given the flows between cells) (Neal et al., 2018). The equations underpinning the
149 model, including their derivation, can be found in Bates et al. (2010) and de Almeida et al. (2012).

150 As input data, *LISFLOOD-FP* requires a DEM (Digital Elevation Model) of the area, channel and boundary condition
151 information (e.g. channel friction, width and depth, hydrograph and evaporation). Flow depth and velocity (for each cell) are
152 the output considered, since they represent the intensity measures of the hazard adopted by this study. The impact of bridges
153 on flow is not explicitly represented in this particular application.

154 **2.2 Computational fluid dynamics (CFD) analysis**

155 Three-dimensional (3D) CFD software is capable of resolving fine details of flood flow around bridges on a local scale such
156 as splashes, eddies, or flow separation, which cannot be captured by depth-averaged methods (such as *LISFLOOD-LP*). Also,
157 bridges present a problem for depth-averaged tools since the computational mesh is two-dimensional and cannot be discretized
158 vertically, which does not allow for a gap underneath a bridge superstructure. To accurately model such behaviors is crucial
159 when estimating flow-induced force demands, which requires the use of a fine, three-dimensional mesh. Additionally, using
160 higher fidelity, three-dimensional models allow for localized loads to be measured on individual faces of a structure, which
161 may be used to determine whether or not individual components fail versus entire structures (Winter et al., 2017).

162 For this study, the three-dimensional CFD code *OpenFOAM* was selected. Flood flows were modelled using the *interFoam*
163 solver, which is a two-phase solver that relies upon Volume of Fluid (VoF) method (Tryggvason et al., 2011) to track the
164 interface between water and air phases. The underlying governing equations that are implemented in *interFoam* are the
165 Reynolds-averaged Navier-Stokes (RANS) equations, which are solved using a predictor-corrector or projection type of
166 method to solve for velocity and pressure fields, and advection equations for the volume fraction introduced by the VoF

167 method. More specifically, pressure-velocity coupling was achieved using the PIMPLE algorithm, which is a combination of
 168 the Pressure-Implicit Split-Operator (PISO) and Semi-Implicit Method For Pressure-Linked Equations (SIMPLE). Since the
 169 RANS system of equations does not constitute a well-posed system due to the so-called Reynolds stress tensor that arises from
 170 the Reynolds-averaging process, a suitable turbulence model that introduces additional equations must be chosen to close the
 171 system. For this study, the $k-\omega$ Shear Stress Transport (SST) model was used due to its ability to handle severely separated
 172 flows near sharp corners better than other similar models such as the Standard, Renormalization Group (RNG), or realizable
 173 $k-\epsilon$ models.

174 2.3 Structural analysis

175 At a minimum, a structural analysis approach should be capable of (i) simulating relevant structural response mechanisms,
 176 which differ based on bridge type, and (ii) characterizing loading derived from the associated CFD model. Finite element (FE)
 177 analysis is commonly employed in structural engineering to simulate the response of bridges to natural hazards for the purpose
 178 of design and performance evaluation. Modern reinforced concrete and steel bridge structures are commonly formed of girders,
 179 cap beams, and pier walls or columns which can be modeled as assemblages of line and spring elements; this approach is
 180 common in practice and can be implemented in a wide variety of structural analysis programs. To model nonlinear response,
 181 which is especially important when considering extreme loads associated with natural hazards, line elements may employ
 182 concentrated or distributed plasticity formulations that make use of nonlinear hinges or fiber sections. Rotational, shear, and/or
 183 axial spring elements can be used to simulate the response of discrete components such as connections and bearings.
 184 Alternatively, continuum finite-element analysis can be employed for members if complex local response of components (e.g.
 185 local buckling and/or deformation) is of interest; this approach is significantly more computationally expensive, however.
 186 Other approaches, such as the discrete-element method, may be well suited for masonry bridges.

187 In this work, modeling with line and spring elements is performed, so this approach will be discussed in greater detail. The
 188 considered bridge consists of a girder superstructure supported on reinforced concrete piers. *OpenSees* (McKenna et al. 2010)
 189 was selected as the analysis software due to its robust nonlinear modeling and scripting capabilities. This latter capability is
 190 beneficial for performance evaluation using a suite of input parameters (in this case, a parameter sweep characterizing different
 191 flood conditions). Moreover, the software is open source and therefore suitable for adaptation in envisioned future work to
 192 enhance interactivity with *OpenFOAM*.

193 Component response and demands based on the structural analysis can be used to assign a damage state for the bridge. Here,
 194 the structural damage is evaluated as slight, moderate, extensive, or complete damage based on the FEMA Hazus manual
 195 (FEMA, 2003). Each of these damage states is associated with level of functionality and repair effort. The qualitative
 196 description of damage states and average repair cost per m^2 (ft^2) is available in literature for hurricanes (Padgett et al., 2008)
 197 and earthquakes (Hazus manual - FEMA, 2003); Gehl and D’Ayala (2018) offered a qualitative damage scale of potential
 198 damage state and failure modes for the bridge components, which could be associated with functionality losses and remedial
 199 actions. Table 1 adapts such literature to riverine flooding using additional works and expert opinion: it lists four identified
 200 damage states (from slight to complete), and associated average repair cost and days of closure due to remedial works (Werner
 201 et al., 2008; Gardoni, 2018; Lam and Adey, 2016).

202 **Table 1. Bridge damage states (Gehl and D’Ayala, 2018) associated to average repair cost per m^2 (Padgett et al., 2008; FEMA, 2003)**
 203 **and average days of closure due to repair (Werner et al., 2008; Gardoni, 2018; Lam and Adey, 2016).**

Damage state	Description	Average repair cost (£/m ²)	Days of closure
Slight	Minor damages such as cracking (shear keys, hinges, deck) and spalling (hinges, columns) that require no more than cosmetic repair.	£1.45/m ² (\$0.25/ft ²)	0-5

	Negligible scour. Some water and/or debris on deck. Full service, likely speed reduction of travelling vehicles.		
Moderate	Moderate experience of shear cracks and spalling that still leave columns structurally sound. Moderate scour and moderate movement of the abutments. Significant water and/or debris on deck. The bridge is partially serviceable (e.g. alternating circulation, reduced capacity and load), but safe to use by emergency vehicles.	£36.54/m ² (\$6.28/ft ²)	5-12
Extensive	Degradation of columns without collapse, shear and cracking leading to structurally unsafety. Significant residual movement at connections or major settlement approach. Delamination failure of individual bearings. Extensive scour of abutments. The bridge is closed to traffic.	£308.66/m ² (\$53.05/ft ²)	13-49
Complete	Collapse of columns or connection losing all bearing support. Imminent deck collapse. Unseating of girders. Scour leading to foundation failure. The bridge is unserviceable.	£1102.77/m ² (\$189.43/ft ²)	>50

204

205 2.4 Fluid-structure coupling

206 The relationship between the CFD and structural analysis is critical to implementation of the proposed framework as outlined
207 in the vulnerability analysis block in Figure 1. Both analyses must adequately represent the bridge geometry, and the CFD
208 output and structural analysis input loading must be compatible. Here, the coupling approach between *OpenFOAM* and
209 *OpenSees* is discussed, but the methodology is applicable to other software. It is noted that *OpenSees* alone is seldom used to
210 model structural response to fluids because of the complexity of the fluid loading and the required coupling mechanism
211 between fluid and solid solvers. As such, the present work is among the first of its kind using *OpenSees*. Other recent research
212 has sought to implement coupling between these multi-physics models. For example, Stephens et al. (2017) demonstrated how
213 *OpenSees* can be “loosely coupled” (i.e., with no interaction between CFD and FE models) with *OpenFOAM* to characterize
214 structural response due to sequential earthquake and tsunami loading. A similar loosely coupled scheme is used here, where:

- 215 i. the bridge superstructure (deck and girders) is modeled as a rigid, 2D cross section with a unit length out of plane and
216 subjected to steady-state flow at different water depths and velocities in *OpenFOAM*;
- 217 ii. the steady-state reactions (output from *OpenFOAM*) on the cross section are recorded; and
- 218 iii. the gravity loads and the steady-state reactions from *OpenFOAM* are applied as distributed, external loads on girder
219 line elements in a 3D *OpenSees* model of the full bridge.

220 It is noted that the bridge superstructure is rigid in the computational fluid dynamics model (an important simplification to
221 facilitate the analysis) but not in the finite-element model.

222 2.5 Impact assessment

223 The impact of a bridge failure in terms of consequences (C) includes direct consequences (C_{dir}) and indirect consequences
224 (C_{ind}), which relate the surrounding transport network (Argyroudis et al., 2019). The total costs C is computed as (Eq. 1):

$$C = C_{dir} + C_{ind} = C_{repair} + C_{cleaning} + C_{detour} + C_{delay} \quad \text{Eq. 1}$$

225 where C_{repair} is the cost associated with repair or replacement of the bridge, C_{clean} is the cost associated with the debris removal
226 (due to flooding), C_{detour} is the additional vehicle operating due to the detour and C_{delay} is the cost associated with trip delays of
227 normal traffic. Indirect costs may also include a fee for closing the bridge that the bridge owner has to pay to transport
228 operators/agencies (e.g. for railways, highways).

229 Table 1 (Sec. 2.3) was functional to compute C_{repair} . Average days of closure due to repairs are obtained via discussion with
230 national operators and existing literature (Werner et al., 2008; Gardoni, 2018; Lam and Adey, 2016). Values for C_{clean} can be
231 researched among historic data of bridge owners, e.g. records from bridge inspection reports. C_{detour} and C_{delay} depend on the
232 network, type of vehicle and traffic flow; this study is limited to consider private cars and HGVs (Heavy Goods Vehicles, i.e.
233 over-3.5-tonnes-gross vehicle weight, including both articulated and rigid body types), for the sake of a contained
234 demonstration. According to standard transport appraisal procedures (e.g. DfT, 2009), the parameters are computed with Eq.
235 2 and Eq. 3 respectively. Considering an origin i , a destination j and a vehicle type z :

236

$$C_{detour} = \sum_i \sum_j \sum_z q_{i,j,z} l_{i,j,z} VOC_z \quad \text{Eq. 2}$$

$$C_{delay} = \sum_i \sum_j \sum_z q_{i,j,z} d_{i,j,z} VTT_z \quad \text{Eq. 3}$$

237

238 q is the volume of traffic, l is the incurred additional length, d is the incurred additional time (delay), VOC is the extra Vehicle
239 Operating Cost (including fuel, tear and wear) and VTT is the Value of Travel Time, i.e. the non-monetary costs incurred along
240 the journey as time spent on transport. The additional length and travel time due to the detour are computed using *ESRI*TM
241 *ArcGIS Network Analyst*, setting the origin and the destination of the trip in opposite sides of the river as demonstration
242 (Pregolato et al., 2016).

243 3 Application and results

244 The city of Carlisle is a flood-prone city (area: 1,040 km²; 2018 population: 108,387) located in the Northwest of England
245 (UK) (Figure 3). Three road bridges connect the two parts of the town over the river Eden from North to South (the A689, A7
246 and M6 bridges) and a fourth one from West to East (Warwick bridge). The 2D hydrodynamic model *LISFLOOD-LP* was set
247 up to simulate a 1-in-500-year flooding scenario (Fig. 3b) for a domain covering 14.75 km² of Carlisle, at 5 m of resolution.
248 This simulation provided flow velocity and inundation height data.

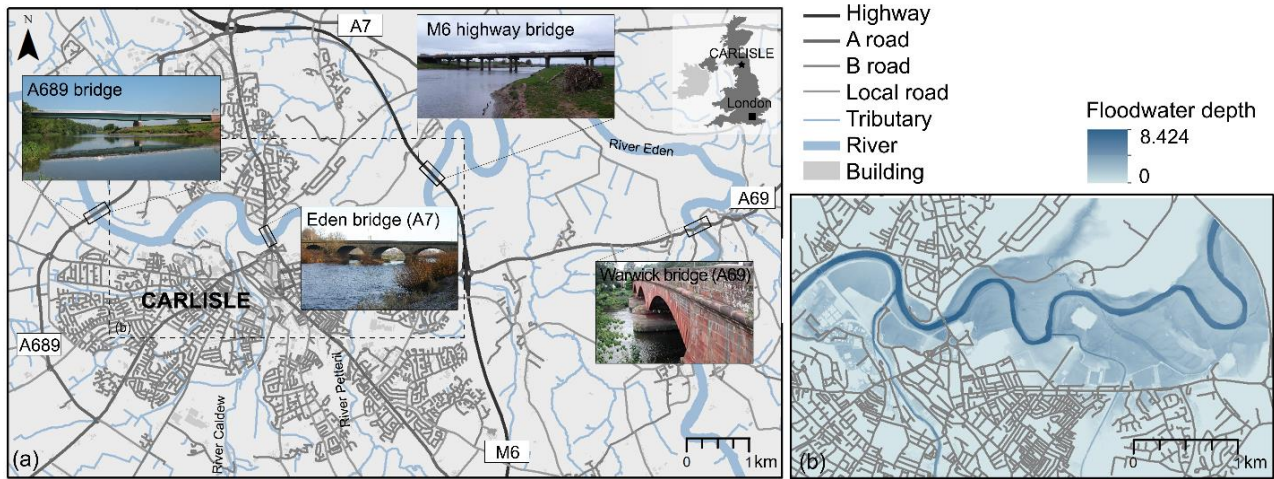
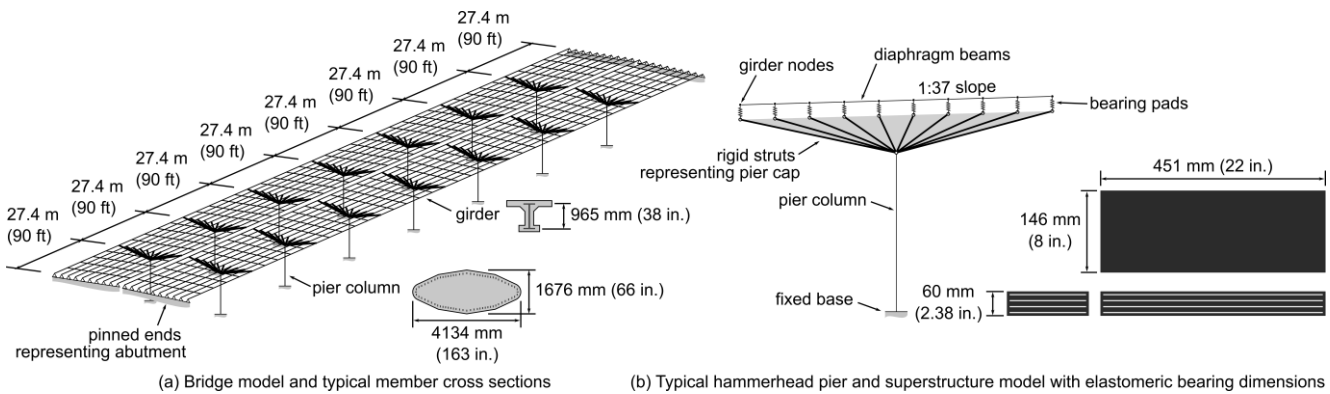


Figure 3. The case study is the city of Carlisle, UK: (a) general overview of Carlisle upon the river Eden, connected North-South by three road bridges (the A689, A7 and M6 bridges) and West-East by the Warwick bridge (A69); (b) flood hazard map for Carlisle, as simulated with LISFLOOD-LP for a 1-in-500-year flood event.

249 As a proof of concept, the M6 highway bridge over the River Eden was considered. The bridge is comprised of a girder
 250 superstructure supported by hammerhead piers. A schematic model of this bridge is shown in Figure 4 with approximate pier
 251 column (reinforced concrete), girder (concrete-encased steel), and bearing pad dimensions.
 252



253 (a) Bridge model and typical member cross sections (b) Typical hammerhead pier and superstructure model with elastomeric bearing dimensions

254 Figure 4. Approximate geometry of M6 bridge as modeled in *OpenSees* including pier column, girder, and bearing dimensions shown
 255 (not to scale).

256 The pier columns are elliptically shaped and oriented to reduce hydraulic drag. The columns taper to a width of 4134 mm and
 257 depth of 1676 mm at the base. The girders are supported on fixed, laminated elastomeric bearing pads with dowels at the
 258 southern end of each span and free spherical bearings at the northern end. Salient bridge and flow input data are summarized
 259 in Table 2.

260
 261 Table 2. Input data of this study for the exemplary CFD analysis of the M6 bridge (Carlisle, UK).

VARIABLE	DATA	SOURCE
Span length	27.4 m	Drawings provided by Highways England
Superstructure width	17.3 m	Drawings provided by Highways England
Superstructure weight (deck, girders, and diaphragm beams)	514 kN/m	Derived from drawings
Flow Velocity	1, 2, and 3 m/s	Modelled (LISFLOOD-LP)
Inundation Height	12.5, 13.0, 13.5, 14.0, 14.5, 15.0, 16.0, 17.0, 18.0 m (from datum; +3.2 m)	Modelled (LISFLOOD-LP)

263 **3.1 CFD simulation and analysis**

264 The CFD simulation was initiated at given inundation heights and flow velocity, as modelled by the *LISFLOOD-LP* model for
 265 a 1-in-a-500-year flood event at the site. The *OpenFOAM* model was set to simulate a range of flow velocity and depth values
 266 above and below the calculated 500-year flood results in order to assess how varying the depth and velocity affected the
 267 resulting bridge performance. Flow velocities and depths were extracted from *LISFLOOD-LP* in proximity of the bridge, and
 268 also compared with historical data overall (e.g., the peak flow recorded at Sheepmount, UK in December 2015 was equal to
 269 $1680.0 \text{ m}^3/\text{s}$; EA, 2016) and inspection reports. The statistics for the velocity (both in its actual flood flow direction and also
 270 normal to the bridge) were computed from the *LISFLOOD-LP* velocity vector (V_x , V_y) and maximum water depth data,
 271 considering maximum values for both quantities over the whole flood simulation. The 500-year return period flood showed
 272 velocity values up to roughly 3.5 m/s and max flood depth up to 17 m near the M6 Bridge. These statistics motivated using a
 273 range of steady-state velocities of 1-3 m/s and inundation elevations of 12.5-18 m above datum in the *OpenFOAM* simulations.
 274 The bridge superstructure was positioned such that the bottom of the bridge's lowest girders and the highest point of the top
 275 of the bridge deck were at elevations of 12.375 m and 14.425 m, respectively, relative to the datum, which was 3.2 m below
 276 the riverbed's lowest point. Flow rates corresponding to the range of selected flow velocities and depths were specified at the
 277 inlet boundary of the *OpenFOAM* model using the `variableHeightFlowrate` boundary condition. To model the free-surface
 278 flow of the Eden River interacting with the M6 bridge in *OpenFOAM*, the `interFoam` multiphase fluid flow solver which
 279 utilizes the Volume of Fluid method for interface tracking was used along with the `k- ω` SST turbulence model to resolve
 280 turbulent flow behaviors. Default *OpenFOAM* values for air-water physical fluid properties (densities: $\rho_{\text{air}} = 1 \text{ kg/m}^3$, $\rho_{\text{water}} =$
 281 1000 kg/m^3 ; kinematic viscosities: $\nu_{\text{air}} = 1.48(10^{-5}) \text{ m}^2/\text{s}$; $\nu_{\text{water}} = 1.0(10^{-6}) \text{ m}^2/\text{s}$; surface tension: $\sigma = 0.07 \text{ N/m}$) and turbulence
 282 model coefficients were used for all simulations. A full summary of all *OpenFOAM* boundary conditions is provided in Table
 283 3.

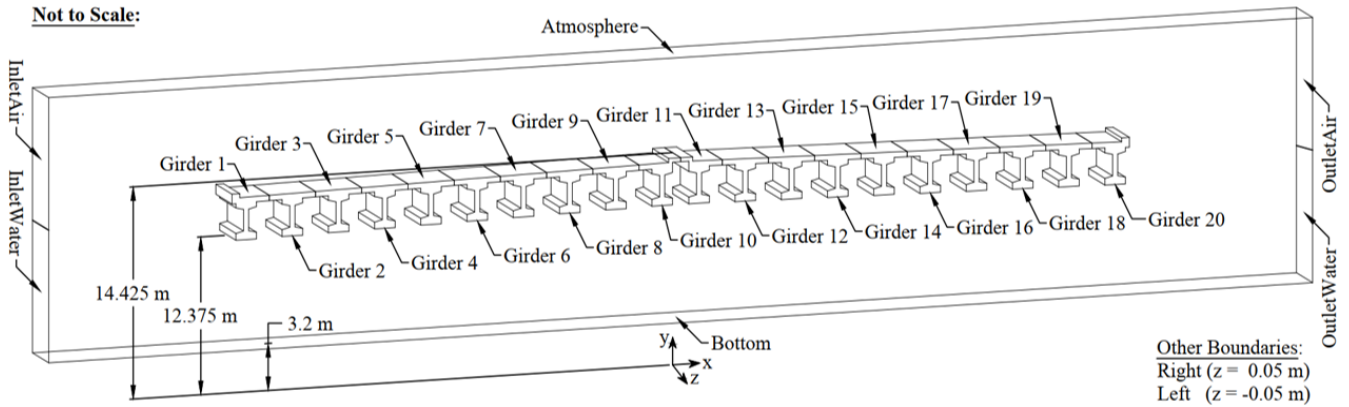
284 **Table 3. *OpenFOAM* model boundary conditions.**

Boundary	OpenFOAM Simulation Field Variables						
	alpha	epsilon	k	nut	omega	p_rgh	U
InletWater	variableHeight-Flowrate	fixedValue	fixedValue	calculated	fixedValue	zeroGradient	variableHeightFlow-RateInletVelocity
InletAir	inletOutlet	inletOutlet	inletOutlet	calculated	inletOutlet	totalPressure	pressureInletOutlet-Velocity
OutletWater	zeroGradient	zeroGradient	zeroGradient	calculated	zeroGradient	zeroGradient	inletOutlet
OutletAir	zeroGradient	zeroGradient	zeroGradient	calculated	zeroGradient	totalPressure	pressureInletOutlet-Velocity
Right	empty	empty	empty	empty	empty	empty	empty
Left	empty	empty	empty	empty	empty	empty	empty
Bottom	zeroGradient	epsilonWall-Function	kqRWall-Function	nutkWall-Function	omegaWall-Function	fixedFlux-Pressure	noSlip
Atmosphere	inletOutlet	inletOutlet	inletOutlet	calculated	inletOutlet	totalPressure	pressureInletOutlet-Velocity
Bridge	zeroGradient	epsilonWall-Function	kqRWall-Function	nutkWall-Function	omegaWall-Function	fixedFlux-Pressure	noSlip

285

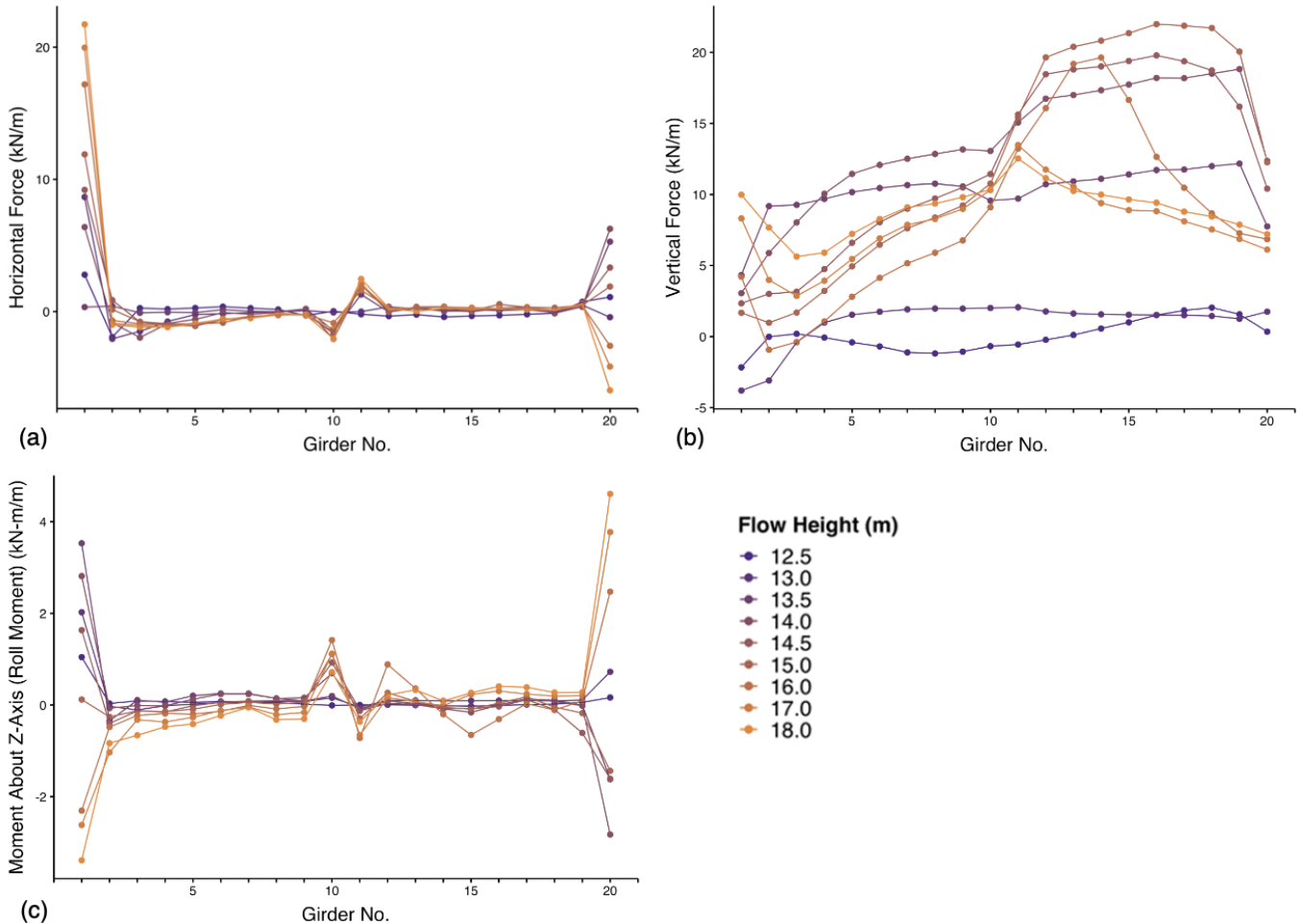
286 To reduce computation time and provide conservative results, a unit width segment of the bridge superstructure located above
 287 the deepest point of the Eden River beneath the M6 Bridge was analyzed in *OpenFOAM*, which resulted in a 2D simulation
 288 that drastically reduced the mesh cell count compared to a full 3D simulation of the entire bridge. Additionally, the out-of-
 289 plane direction components of the flow were neglected in all simulations by using the empty type of *OpenFOAM* boundary
 290 condition, ensuring the simulations were truly 2D. This setting allowed for more simulations to be run using a wider range of

291 flooding conditions in less time while conducting the parametric study. As shown in Fig. 5, the model measured forces on 20
 292 individual components along the cross-section of the bridge superstructure segment corresponding to each girder and its
 293 tributary width of the bridge deck.



294
 295 **Figure 5. OpenFOAM Model Geometry and Boundary Conditions**

296
 297 Fig. 6 shows examples converged outputs from the discussed simulations for an initial flow velocity equal to 3 meters per
 298 second for all individual components and initial inundation levels. Values are expressed per meter of bridge deck width, as
 299 extended from the 2D simulations.



300
 301 **Figure 6. Converged simulated component loads for flow velocity equals 3 meters/second per girder component; (a) shows horizontal**
 302 **(x-direction) loads applied in kN per meter bridge width; (b) shows vertical (y-direction) loads applied in kN per meter bridge width;**
 303 **(c) shows moment about the z-axis (i.e. roll moment) in kN-m per meter bridge width.**

304

305 3.2 Structural analysis and damage assessment

306 The *OpenSees* model was developed using fiber-based line elements for the reinforced-concrete pier columns and preflex
307 girders (a form of prestressed, concrete-encased steel beams). Nonlinear concrete (Concrete02) and steel (Steel02) constitutive
308 models were employed to simulate uniaxial material response in the fibers. All concrete was assumed to have a compressive
309 strength of 34.5 MPa. The steel reinforcement and encased structural steel was assumed to have yield stresses of 276 MPa and
310 379 MPa, respectively. The girders ends were connected to pier caps (modeled as rigid) via linear-elastic springs to represent
311 bearings. The free spherical bearings were modeled as roller boundary conditions. The steel-laminated elastomeric bearing
312 pads were modeled with lateral, vertical, rotational, and torsional stiffnesses based on linear theory of bearings as described
313 by Stanton et al. (2008). The elastomeric bearing dimensions are shown in Figure 4; each had two, 13-mm-thick layers of
314 elastomer reinforced with 3-mm steel plates. The elastomer was assumed to have a bulk modulus of 3100 MPa and a shear
315 modulus of 0.76 MPa; the bearing dimensions and material properties led to the stiffness parameters defined in Table 4. The
316 bearing spring elements were connected to rigid links which simulated pier cap beams, providing a load path between the
317 girders and pier columns. The bridge abutments were founded on rock on the north side and piles on the south side; both
318 abutments were modeled as rigid. The piers were founded on rock and pier columns were modeled as fixed. It is noted that
319 many bridge foundations are vulnerable to scour, especially under flood conditions; however, the piers and abutments of the
320 considered bridge are founded on rock, thus scour is not a concern for this structure (and in general scour and soil-structure
321 interaction effects are beyond the scope of the present work).

322

323 **Table 4. OpenSees Elastomeric Bearing Spring Stiffnesses**

Stiffness type	Direction	Value
Axial	—	142 kN/mm
Shear	—	1.69 kN/mm
Rotational	Deformation in short-axis direction	311 kN-m/rad
	Deformation in long-axis direction	2350 kN-m/rad
Torsional	—	17.9 kN-m/rad

324

325 To analyze the bridge, gravity loads were first applied based on the self-weight of the structural components; no live loads
326 were considered. The lateral forces, vertical forces, and roll moments determined from *OpenFOAM* were then applied as
327 distributed loads in *OpenSees* on each bridge girder (i.e., over all eight spans with 20 girders per span); this is the key link
328 between the CFD and structural models.

329 Under the range of loading investigated, yielding or cracking was not detected in the girders or columns, and the simulated
330 hydraulic forces were not large enough to overcome the self-weight of the structure, which would result in uplift of the
331 superstructure. However, the elastomeric bearing pads sustained large shear demands near the design limits specified by
332 Section 14.7.5 of the AASHTO *LRFD Bridge Specification* (2017). Specifically, the elastomeric bearings were evaluated for:

- 333 i. loss of frictional resistance between the bearing and girder based on the ratio of shear and normal forces on the
334 bearings,
- 335 ii. excessive shear deformation, and
- 336 iii. excessive shear strain due to combined axial load, rotation, and shear deformation.

337 The solid lines in Figure 7 compare maximum shear forces, deformations, and strains in any of the elastomeric bearings for
338 each of the loading scenarios investigated; Figures 7a, 7c, and 7e show these engineering demand parameters versus flow
339 velocity and Figures 7b, 7d, and 7f show corresponding values with respect to flow height. The data suggest that peak steady-
340 state demands on any of the elastomeric bearings in the bridge occur around a flow height 15 m, at which point the bridge has
341 just reached full inundation. In addition, below a flow height of 15 m, demands consistently increase with velocity; such

342 increases in demand after full inundation are not consistently observed, which suggests that the loading is primarily associated
 343 with hydrodynamic effects that are a function of the effective area of the cross-section, and may also be affected by the fact
 344 that the flow around the superstructure is less turbulent. To expand the data set, linear extrapolation to flow velocities of up to
 345 6 m/s are shown in Figures 7a, 7c, and 7e as dotted lines with open markers. It is noted that the plots in Figure 7 show peak
 346 demands across all elastomeric bearings in the bridge, and the actual extent of damage depends on the progression of failure
 347 in multiple bearings.

348 The Commentary to the AASHTO *LRFD Bridge Specification* (2017) states a coefficient of friction of 0.2 between elastomeric
 349 bearings and concrete is appropriate for design, and this limit is used here to evaluate potential girder unseating due to loss of
 350 frictional resistance. For the purpose of this evaluation, dowel resistance is neglected, though this could prevent unseating in
 351 practice. Figures 7a and 7b plot the peak ratios of shear-to-normal forces across all bearings on the bridge, and it can be
 352 observed that the bearings are well below the limit suggested in the AASHTO Commentary, which is labeled as μ_{max} and
 353 shown as the grey line. However, it must be noted that the coefficient of friction may be lower than expected under wet
 354 conditions and that the lateral hydrodynamic loading can be significant, increasing vulnerability of unseating due to debris
 355 impact. To illustrate how the sequential fluid-structure modeling results may be applied, a highly conservative, reduced
 356 coefficient friction of 0.1 is considered. Using this threshold, the results indicate flow conditions for which the given frictional
 357 resistance is approached or exceeded: 13.5-m flow depth with velocity of at least 6 m/s, 15-m flow depth with velocity of at
 358 least 5 m/s, 18-m flow depth with velocity of at least 6 m/s.

359 Figures 7c and 7d show peak shear strains due to loading perpendicular to the short edge of the bearing pad (see Figure 4b)
 360 due to combined axial load (γ_a), rotation (γ_r), and shear (γ_s). The shear strains are computed based on Eqs. 4-6 based on the
 361 AASHTO *LRFD Bridge Specification* (2017).

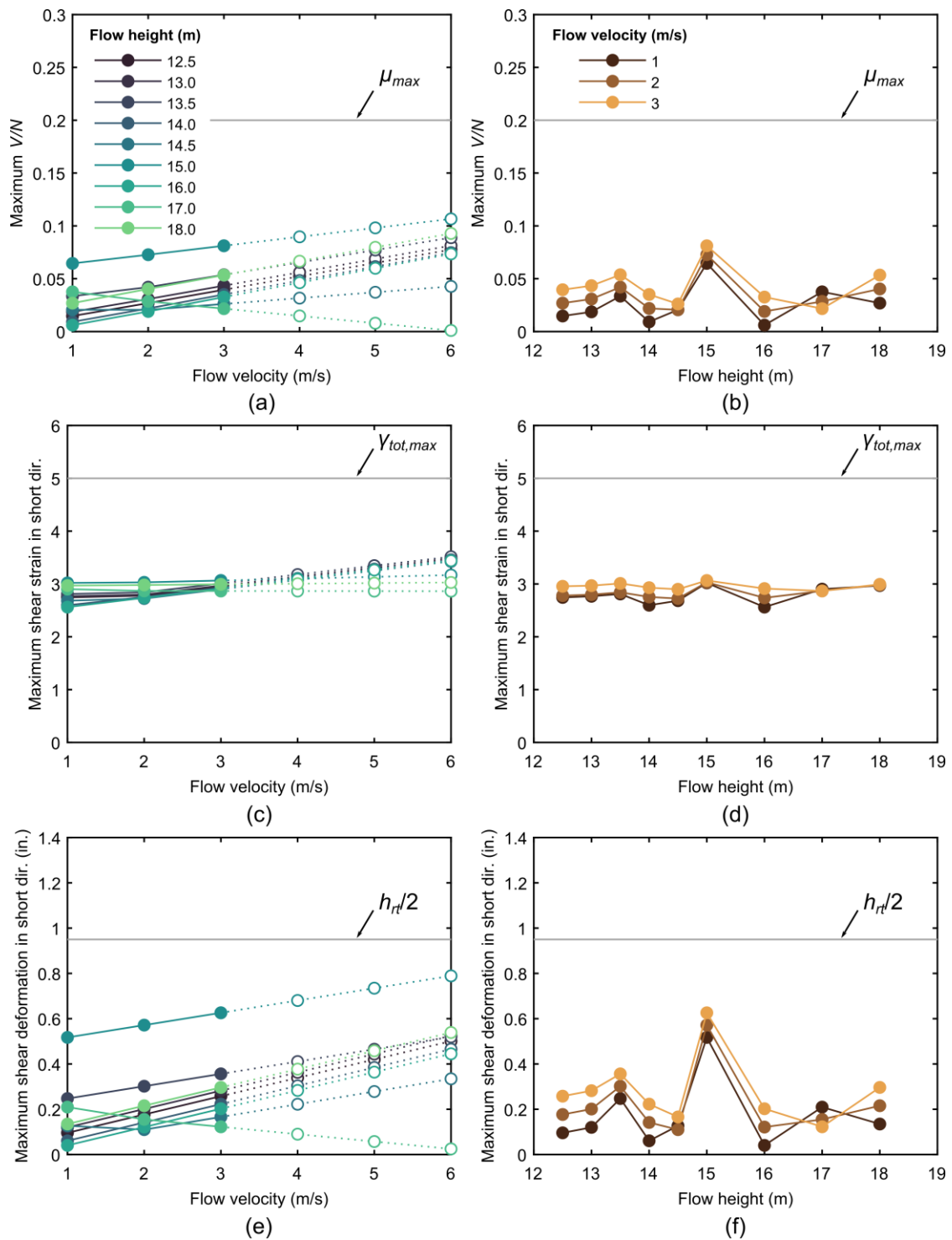
$$\gamma_a = D_a \frac{\sigma_s}{G S_i} \quad \text{Eq. 4}$$

$$\gamma_r = D_r \left(\frac{L}{h_{ri}} \right)^2 \frac{\theta_s}{n} \quad \text{Eq. 5}$$

$$\gamma_s = \frac{\Delta_s}{h_{rt}} \quad \text{Eq. 6}$$

362 In the above equations, D_a and D_r are empirical coefficients, σ_s is the average compressive stress, G is the shear modulus, S_i
 363 is the shape factor of the i^{th} internal layer, L is the bearing length perpendicular to the axis of rotation, h_{ri} is the thickness of
 364 the i^{th} internal elastomeric layer, h_{rt} is the total thickness of the elastomer, θ_s is the rotation demand, n is the number of interior
 365 elastomeric layers, and Δ_s is the shear deformation. Note that σ_s , θ_s , and Δ_s are outputs from the structural analysis; the
 366 rotation demand, θ_s , includes 0.005 rad of rotation due to misalignment. For design per the AASHTO *LRFD Bridge*
 367 *Specification* (2017), the combined shear strain due to these actions should not exceed 5.0, and this criterion is satisfied in the
 368 analyses (all values, including extrapolated values, are below the grey line in Figures 7c and 7d).

369 The shear deformation demand on the bearing, Δ_s , is shown to be more critical than the combined shear strains: Figures 7e
 370 and 7f show these data with the annotated shear strain limit of $h_{rt}/2$ in grey; this limit is also based on the AASHTO
 371 *Specification* (2017). The demand is clearly largest for a flow height of 15 m, and it increases linearly with the flow velocity.



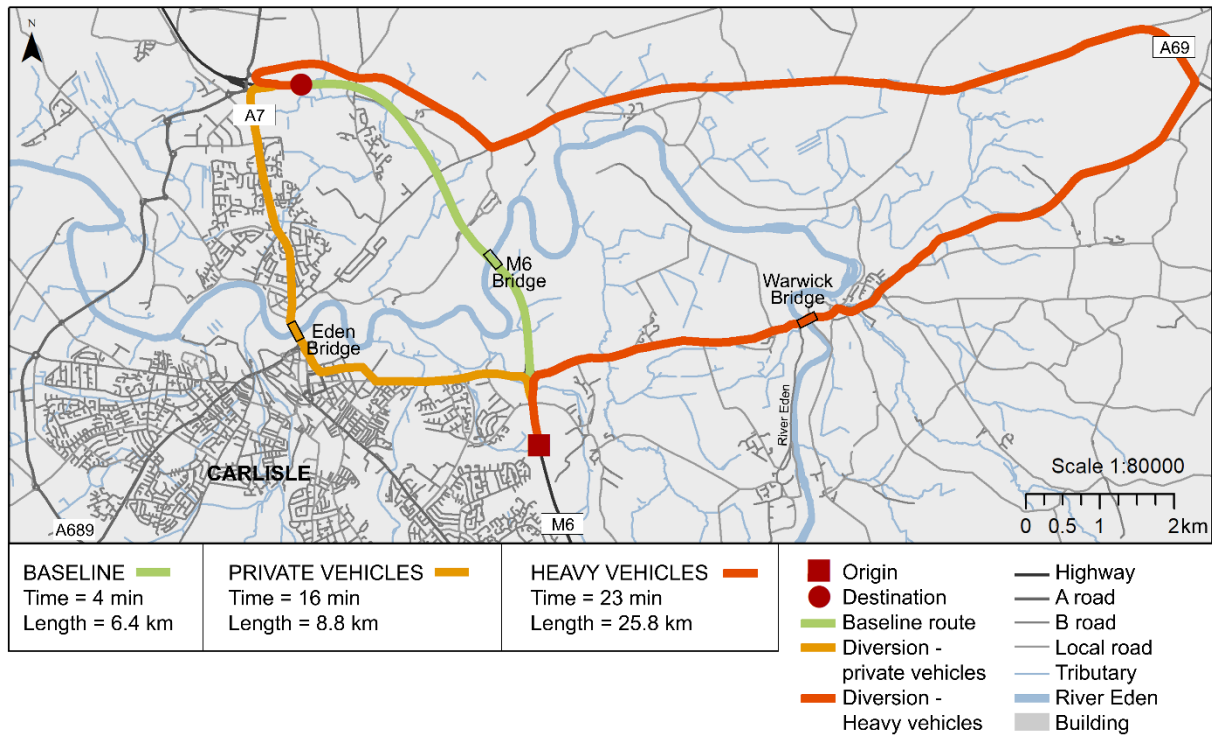
372

373 **Figure 7. Maximum simulated demand on elastomeric bearings in M6 bridge, including (a)/(b) shear force, (c)/(d) total shear strain**
 374 **due to combined axial, moment, and shear demands, and (e)/(f) shear deformation; plots on left show demand versus flow velocity**
 375 **and plots on right show demand versus flow height.**

376 3.3 Network impact and consequence assessment

377 The results of the loosely coupled CFD and structural analyses described above suggest a potential for either girder unseating
 378 due to loss of frictional resistance or excessive shear deformation, which may lead to debonding and delamination for this
 379 particular bridge. In addition, damage associated with these limit states is most expected at a flow height of 15 m and flow
 380 velocity of at least 5 m/s. The impact of damage in this flood scenario is therefore considered in this section. Based on Table
 381 1, the damage state is estimated as moderate because: (i) the bearings approach but do not exceed limit states, (ii) scour is
 382 assumed to be insignificant compared to damage to the superstructure and bearings, and (iii) water overtops the bridge deck.
 383 A moderate damage state implies the bridge closure for 5-12 days (see Table 1). In the case of the M6 bridge, its closure causes

384 disruptions to all southbound and northbound users that are travelling along the M6 (Figure 8). Compared to the baseline
 385 journey, results show that private cars are delayed by 12 minutes and have additional ca. 9 km due to rerouting. HGVs cannot
 386 travel via the historic Eden Bridge (city center) and are subjected to a longer rerouting, which leads to 19 minutes and ca. 20
 387 km of delay and additional travelling respectively.



388
 389 **Figure 8. Routes for crossing the river Eden along the highway in baseline and disrupted conditions; private and heavy vehicles are**
 390 **rerouted on different journeys when the M6 bridge is disrupted.**

391 The cost of the impact due to the M6 bridge disruption is computed in terms of direct and indirect consequences using Eq. 1;
 392 output and input values are specified in Table 5.

393 **Table 5. Output and input data for the impact cost calculation considering disruption due to an extreme flood event on the M6**
 394 **bridge in Carlisle. Acronyms: VTT – Value of Travel Time; HGV - Heavy Good Vehicle; VOC – Vehicle Operating Cost; ADT -**
 395 **Average Daily Traffic.**

	VARIABLE	DATA	SOURCE
INPUT	Average repair cost (£/m ²)	£36.54/m ²	Table 1
	Time for repairs (T_{repair})	7 days	Table 1
	VTT for HGVs	£10.10/hour	DfT (2009)
	Delay for HGVs	19 min	computed
	Detour length for HGVs	19.4km	computed
	VOC for HGVs	37.668 p/km	Blakemore (2018)
	ADT for HGVs	1833 veh/day	UK national statistics
	VTT for average private vehicles	£6.81/hour	DfT (2009)
	Delay for average private vehicles	12 min	computed
	Detour length for private vehicles	2.4 km	computed
	VOC for private vehicles	25.47p/km	Yurday (2020)
	ADT for average private vehicles	28602 veh/day	UK national statistics
OUT	C_{repair}	£7,308.00	computed
	C_{clean}	£29,476.00	Panici et al. (2020)

	C_{detour}	£30,878.65/day	computed
	C_{delay}	£44,818.47/day	computed
TOTAL		£566,663.81	

396

397 The values of Value of Travel Time (VTT) of HGVs (Heavy Good Vehicles, working condition) and average private cars
398 (unspecified conditions) can be found in the UK Department for Transport (DfT) appraisal methods, illustrated in the Cost
399 Benefit Analysis (COBA) manual (DfT, 2009). Data regarding the additional travel time for rerouting has been computing via
400 transport model (Sec. 2.5) and verified with Google Maps (Figure 8); for the UK, topological road network links are freely
401 available nationwide. Data regarding Average Daily Traffic (ADT) flow are freely available
402 (<http://webtris.highwaysengland.co.uk/>) and were obtained by considering the annual northbound and southbound flows for
403 the relevant sites (36,670 veh/day: Site 9538/2 on link M6 southbound and Site 9540/2 on link M6 northbound; 2019 data),
404 considering the traffic composition at 78% for private cars and 5% for HGVs (DfT, 2019).

405 The repair cost (C_{repair}) was computed using Table 1 and assuming 7 days (average) of bridge closure; the cost of debris
406 removal was obtained by looking at the highest cost for a single event in the UK (Panici et al., 2020), since the simulated
407 flooding is an extreme and rare event. The additional vehicle operating due to the detour per day (C_{detour}) was calculated using
408 Eq. 2; the cost associated with trip delays (C_{delay}) was calculated using Eq. 3.

409 For the case study undertaken (Carlisle, UK; 1-in-a-500-ys event), the total cost of the flood impact to the bridge is
410 £566,663.81, considering seven days of bridge closure. The largest proportion (93.5%) of this cost is due to the indirect cost
411 of rerouting traffic (£75,697.12 per day of closure, i.e. £529,879.81); the 6.5% of the total cost is due to direct damages only
412 (£36,784.00).

413 4 DISCUSSION AND FUTURE RESEARCH

414 This study developed an integrated method that uses a multiphysics, multilevel approach for assessing the effect of flooding
415 hazards on a local transportation network. For the city of Carlisle (UK), a 1-in-500-years flooding event was simulated and
416 the resulting hydrodynamic forces on the highway bridge (M6) modelled. While simulated hydrodynamic forces and Finite
417 Element (FE) analysis did not show uplift failure, overtopping of the bridge is shown to occur at inundation heights of 14 m
418 and above. Given the potential for flood-related disruption of traffic, overtopping should be considered temporary network
419 failure in its own right. The elastomeric bearings supporting the bridge girders approached shear deformations near design
420 limits at a flow height of 15 m, and a potential loss of frictional resistance between the elastomer and concrete is also observed.
421 While these limit states were not exceeded for flow velocities up to 3 m/s, extrapolation to faster flow rates suggests higher
422 potential for damage. This notwithstanding, the bridge would lose immediate functionality at a flow height of between 13.5
423 and 14.0 m due to inundation of the deck even if the structure sustains no damage. The impact analysis showed that indirect
424 damages covered the 93.5% of the total cost of damages to the bridge, proving that limiting the assessment to repairs and
425 debris cleaning would greatly underestimate the impact of flooding to bridges.

426 The produced outputs are conceptual results and thus approximate and indicative for multiple reasons. First, there is a dearth
427 of UK-specific data regarding bridge repairs, duration time of repair, etc.; research or survey to solicit post-flood data are
428 highly recommended to improve impact estimates. For example, a bridge could be partially closed during repairs (according
429 to its damage state) and allow traffic in one direction. Second, the modeling approach presented herein used several intentional
430 simplifications for demonstration purposes, including reducing the CFD domain, neglecting soil-foundation effects and scour
431 modeling, and assumed rigidity of the structural system among others. In scenarios where these issues (or others) may be of
432 more concern for a particular bridge, the fidelity of the modeling approach could be improved. Additionally, the failure states
433 presented here may not translate broadly to the general bridge inventory, but additional or alternative structural/functional

434 failure states could be applied. Third, the impact analysis was limited to private cars and HGVs for demonstration purposes;
435 however, advanced transport appraisal could better capture users' choices and the engineering response of lifelines by
436 including a wider range of vehicles categories and traffic scenarios. In terms of impact, the presence of floodwater on the roads
437 is not simulated for limiting the focus of this work on riverine flooding and the bridge impact consequences; for properly
438 analyzing the flooding impact to road networks, simulation of surface water flooding should be undertaken; this analysis would
439 be a study on its own, and currently out of the scope of this piece of research. Flood impact on other parts of the network would
440 limit the capacity of the alternative routes, causing additional delays to the traffic; thus, obtained results represent an
441 underestimation of the overall systemic cost. Nevertheless, the proposed approach of impact analysis can give community
442 leaders a comprehensive method for assessing susceptibility to flooding and relative consequences at systemic level and the
443 case study presented here represents an archetype for this approach.

444 Thus, the importance of this study consists in the proof of concept of a new holistic methodology which uses a multilevel
445 approach to improve the fidelity of network failure predictions, taking advantage of seemingly disparate physical models. The
446 computed hydrodynamic forces were applied directly into a traditional FE model to predict the global structural response to
447 identify critical structural components and damage states. Notably, the hydrodynamic forces induced large demands on
448 bearings that are often not considered in design. Because of the critical nature of bridges to a transportation network, the impact
449 analysis revealed that indirect cost cover almost all the total cost due to flooding; this consideration is fundamental for
450 infrastructure owners and managers when managing assets and budgets.

451 Next steps of this study will analyze the impact of the closure for a second bridge (e.g. the masonry arch Eden Bridge), in
452 isolation first and then in combination with the M6 bridge. Future work should investigate the impacts of other limit states
453 which could result in total or partial bridge closure; a wider range of bridge types should be investigated too. Such analyses
454 would benefit from 3D CFD and FE models to help refining demands on the structure and reducing uncertainty in the predicted
455 bridge performance. Ultimately, this approach can be applied to any coastal or riverine structure where large-scale water
456 inundation is expected.

457 **5 CONCLUSION**

458 This study focused on riverine bridges prone to failures during flood events. This study established rigorous practices of
459 Computational Fluid Dynamics (CFD) for modelling hydrodynamic forces on inundated bridges, and understanding the
460 consequences of such impact on the surrounding network. The hydrodynamic forces were modelled as demand on the bridge
461 structure and inputted into a vulnerability analysis of the structure; the performance evaluation s showed a moderate damage
462 state of the bridge which was used to approximate the overall direct and indirect consequences. For the city of Carlisle (UK)
463 and a 1-in-500-years flooding, results showed that the flood impact to the M6 bridge (highway bridge) caused more than £500k
464 of damages of which 93.5% indirect damages (rerouting and delays). The relevance of this work resides in the integrated
465 method that couple practices of CFD with performance and network analysis, which allows to estimate the cost due to flooding
466 impact to a bridge considering the surrounding transport system. Infrastructure owners and managers, as well as modelers and
467 researchers, should build on this work to better predict local fluid pressures that may lead to bridge structural failure and related
468 network economic consequences.

469 **DATA AVAILABILITY STATEMENT**

470 All relevant and publicly available data will be shared via the DataBris repository of the University of Bristol if the paper will
471 be accepted for publication; data sources are clearly specified throughout the paper.

472 **ACKNOWLEDGEMENTS**

473 MP was supported by the Engineering and Physical Sciences Research Council (EPSRC) LWEC (Living With Environmental
474 Change) Fellowship (EP/R00742X/1 and 2). The authors also grateful acknowledge: Mark Pooley at Highways England; John
475 L. Kelsall at Phoenix Architecture & Planning; Mohammad Fereshtehpour at Ferdowsi University of Mashhad.

476 **References**

- 477 AASHTO: Standard specifications for highway bridges, 7th Edition, Washington, DC, 2002.
- 478 AASHTO: AASHTO LRFD Bridge Design Specifications; 8th Edition, Washington, DC, 2017.
- 479 Ahamed, T., Duan, J. G., Jo, H.: Flood-fragility analysis of instream bridges—consideration of flow hydraulics, geotechnical
480 uncertainties, and variable scour depth. *Structure and Infrastructure Engineering*, 1-14,
481 <https://doi.org/10.1080/15732479.2020.1815226>, 2020.
- 482 Argyroudis, S.A., Mitoulis, S.A., Winter, M.G., Kaynia A.M.: Fragility of transport assets exposed to multiple hazards: State-
483 of-the-art review toward infrastructural resilience, *Reliability Engineering & System Safety* 191, 106567,
484 <https://doi.org/10.1016/j.res.2019.106567>, 2019.
- 485 Arneson, L.A., Zevenbergen, L.W., Lagasse P.F., Clopper, P.E.: Evaluating scour at bridges, 5th Edition, Publication no.
486 FHWA-HIF-12-003, Hydraulic Engineering Circular No. 18. U.S. Department of Transportation, Federal Highway
487 Administration, 2012.
- 488 Arrighi C., Pregolato M., Dawson R., Castelli F.: Preparedness against mobility disruption by floods, *Science of the Total*
489 *Env.*, 654: 1010-1022, <https://doi.org/10.1016/j.scitotenv.2018.11.191>, 2019.
- 490 Bates P.D., Horritt M.S. and Fewtrell T.J.: A simple inertial formulation of the shallow water equations for efficient two-
491 dimensional flood inundation modelling, *J. Hydrol.* 387(1–2): 33-45. doi: 10.1016/j.jhydrol.2010.03.027, 2010.
- 492 Blakemore T.: Truck operating costs report for 2018: <https://thetruckexpert.co.uk/truck-operating-costs-report-for-2018/> last
493 access: 12 May 2020, 2018.
- 494 Carey T.J., Mason H.B., Barbosa A.R., Michael H.S.: Multihazard Earthquake and Tsunami Effects on Soil–Foundation–
495 Bridge Systems, *J. Bridge Eng.*, 24(4), 04019004, doi: [https://doi.org/10.1061/\(ASCE\)BE.1943-5592.0001353](https://doi.org/10.1061/(ASCE)BE.1943-5592.0001353), 2019
- 496 Department for Transport (DfT): COBA Manual: [https://www.gov.uk/government/publications/cobalt-software-and-user-](https://www.gov.uk/government/publications/cobalt-software-and-user-manuals)
497 [manuals](https://www.gov.uk/government/publications/cobalt-software-and-user-manuals), last access: 12 May 2020, 2009.
- 498 Department for Transport (DfT): Road Traffic Estimates: Great Britain 2018:
499 [https://assets.publishing.service.gov.uk/government/uploads/system/uploads/attachment_data/file/808555/road-traffic-](https://assets.publishing.service.gov.uk/government/uploads/system/uploads/attachment_data/file/808555/road-traffic-estimates-in-great-britain-2018.pdf)
500 [estimates-in-great-britain-2018.pdf](https://assets.publishing.service.gov.uk/government/uploads/system/uploads/attachment_data/file/808555/road-traffic-estimates-in-great-britain-2018.pdf), last access: 12 May 2020, 2019.
- 501 de Almeida G.A.M., Bates P.D., Freer J.E., Souvignet M.: Improving the stability of a simple formulation of the shallow water
502 equations for 2-D flood modelling, *Water Resour. Res.*, 48(5), W05528, doi: 10.1029/2011wr011570, 2012.
- 503 EA: Carlisle Flood Investigation Report 2016. Environment Agency (EA), Cumbria County Council:
504 <https://www.cumbria.gov.uk/planning-environment/flooding/flood-investigation-reports-carlisle.asp>, last access: 12
505 November 2020, 2016.
- 506 Ertugay K., Argyroudis S. and Düzgün H.Ş.: Accessibility modeling in earthquake case considering road closure probabilities:
507 a case study of health and shelter service accessibility in Thessaloniki, Greece, *Int. J. of Disaster Risk Reduction*, 17, 49–
508 66, <https://doi.org/10.1016/j.ijdrr.2016.03.005>, 2016.
- 509 Gardoni, P.: *Routledge Handbook of Sustainable and Resilient Infrastructure*. London, Routledge,
510 <https://doi.org/10.4324/9781315142074>, 2018.

511 Gidaris, I., Padgett, J. E., Barbosa, A. R., Chen, S., Cox, D. T., Webb, B. and Cerato, A.: Multiple-hazard fragility and
512 restoration models of highway bridges for regional risk and resilience assessment in the United States: State-of-the-art
513 review, *J. Struct. Eng.* 143 (3), 04016188, [https://doi.org/10.1061/\(ASCE\)ST.1943-541X.0001672](https://doi.org/10.1061/(ASCE)ST.1943-541X.0001672), 2017.

514 Gehl, P. and D'Ayala, D.: System loss assessment of bridge networks accounting for multi-hazard interactions. *Structure and*
515 *Infrastructure Engineering*, 14(10), 1355-1371, 2018.

516 Grossi, P. and Kunreuther, H.: *Catastrophe Modeling: A New Approach to Managing Risk*, New York, Springer-Verlag, 2005.

517 FEMA: HAZUS-MH MR1: Technical manual, Earthquake Model, Federal Emergency Management Agency, Washington,
518 D.C., 2003.

519 Highways England (HE): Design Manual for Roads and Bridges BD 97/12 The assessment of scour and other hydraulic actions
520 at highway structures: <http://www.standardsforhighways.co.uk/ha/standards/dmrb/vol3/section4/bd9712.pdf>, last access:
521 12 May 2020, 2012.

522 Hung, C. C., Yau, W. G.: Vulnerability evaluation of scoured bridges under floods. *Engineering Structures*, 132, 288-299,
523 2017.

524 Hunt, B.: *Monitoring scour critical bridges* (Vol. 396). Washington, DC: Transportation Research Board, 2009

525 Johnson, P.A., Whittington, R.M.: Vulnerability-based risk assessment for stream instability at bridges. *Journal of Hydraulic*
526 *Engineering*, 137(10), 1248-1256, [https://doi.org/10.1061/\(ASCE\)HY.1943-7900.0000443](https://doi.org/10.1061/(ASCE)HY.1943-7900.0000443), 2011

527 Kerényi, K., Sofu, T. and Guo: J. Hydrodynamic forces on inundated bridge decks, Federal Highway Administration, FHWA-
528 HRT-09-028, 2009.

529 Khan, M. A.: Rapid Bridge Insertions Following Failures. Chapter 6. *Accelerated Bridge Construction*, Butterworth-
530 Heinemann, 257-308, ISBN 9780124072244. <https://doi.org/10.1016/B978-0-12-407224-4.00006-X>, 2015

531 Kilanitis, I. and Sextos, A.: Integrated seismic risk and resilience assessment of roadway networks in earthquake prone areas,
532 *Bulletin of Earthquake*, 17, 181–210, <https://doi.org/10.1007/s10518-018-0457-y>, 2019.

533 Kim, H., Sim, S. H., Lee, J., Lee, Y. J., Kim, J. M.: Flood fragility analysis for bridges with multiple failure modes. *Advances*
534 *in Mechanical Engineering*, 9(3), 1687814017696415, 2017.

535 Kirby, A. M., Roca, M., Kitchen, A., Escarameia, M. and Chesterton, O. J.: *Manual on scour at bridges and other hydraulic*
536 *structures*, 2nd edition, CIRIA C742, RP987, London, CIRIA, ISBN: 978-0-86017-747-0, 2015.

537 Lam, J. C. and Adey, B. T.: Integrating functional loss assessment and restoration analysis in the quantification of indirect
538 consequences of natural hazards, *ASCE-ASME J. Risk and Uncertainty in Eng. Systems*, Part A: Civil Engineering, 2:
539 04016008, <https://doi.org/10.1061/AJRUA6.0000877>, 2016.

540 Liu, L., Frangopol, D.M., Mondoro, A. and Yang, D.Y.: Sustainability-Informed Bridge Ranking under Scour Based on
541 Transportation Network Performance and Multi-attribute Utility. *J. Bridge Eng.*, 23(10), 04018082,
542 [https://doi.org/10.1061/\(ASCE\)BE.1943-5592.0001296](https://doi.org/10.1061/(ASCE)BE.1943-5592.0001296), 2018.

543 Lomonaco, P., Alam M. S., Arduino, P., Barbosa, A., Cox, D.T., Do, T., Eberhard, M., Motley, M.R., Shekhar, K., Tomiczek,
544 T., Park, H., van de Lindt, J.W. and Winter, A.: Experimental modeling of wave forces and hydrodynamics on elevated
545 coastal structures subject to waves, surge or tsunamis: the effect of breaking, shielding and debris, *Coastal Eng. Proceedings*
546 1 (36), 53, <https://doi.org/10.9753/icce.v36.waves.53>, 2018.

547 McKenna, F., Scott, M.H., and Fenves, G.L.: Nonlinear finite-element analysis software architecture using object composition,
548 *J. Comput. Civ. Eng.* 24: 95-107, 2010.

549 Mondoro, A. and Frangopol, D.M.: Risk-based cost-benefit analysis for the retrofit of bridges exposed to extreme hydrologic
550 events considering multiple failure modes, *Eng. Struct.*, 159, 310-319, <https://doi.org/10.1016/j.engstruct.2017.12.029>,
551 2018.

552 Motley, M.R., Wong, H.K., Qin X., Winter, A.O. and Eberhard, M.O.: Tsunami-induced forces on skewed bridges, *J.*
553 *Waterway, Port, Coastal, Ocean Eng.* 142(3), 04015025, [https://doi.org/10.1061/\(ASCE\)WW.1943-5460.0000328](https://doi.org/10.1061/(ASCE)WW.1943-5460.0000328), 2016.

554 Neal, J.C., Bates, P.D., Fewtrell, T.J., Hunter, N.M., Wilson, M.D. and Horritt, M.S.: Distributed whole city water level
555 measurements from the Carlisle 2005 urban flood event and comparison with hydraulic model simulations, *J. Hydrol.*,
556 368(1–4), 42-55, <https://doi.org/10.1016/j.jhydrol.2009.01.026>, 2009.

557 Neal, J.C, Dunne, T., Sampson, C., Smith, A. and Bates, P.D.: Optimisation of the two-dimensional hydraulic model
558 LISFLOOD-LP for CPU architecture, *Environ. Model. Softw.*, 107, 148-157,
559 <https://doi.org/10.1016/j.envsoft.2018.05.011>, 2018

560 Oudenbroek, K., Naderi, N., Bricker, J.D., Yang, Y., Van der Veen, C., Uijttewaal, W., Moriguchi, S. and Jonkman, S.N.:
561 Hydrodynamic and Debris-Damming Failure of Bridge Decks and Piers in Steady Flow, *Geosciences*, 8 (11), 409,
562 <https://doi.org/10.3390/geosciences8110409>, 2018..

563 Padgett, J.E., DesRoches, R., Nielson, B., Yashinsky, M., Kwon, O.-S., Burdette, M. and Tavera E.: Bridge damage and repair
564 costs from hurricane Katrina, *J. Bridge Eng.*, 13(1), 6-14, [https://doi.org/10.1061/\(ASCE\)1084-0702\(2008\)13:1\(6\)](https://doi.org/10.1061/(ASCE)1084-0702(2008)13:1(6)), 2008.

565 Panici, D., Kripakaran, P., Djordjević, S. and Dentith, K.: A practical method to assess risks from large wood debris
566 accumulations at bridge piers, *Science of The Total Environment*, 728, 138575,
567 <https://doi.org/10.1016/j.scitotenv.2020.138575>, 2020

568 Pregnolato, M., Vardanega, P.J., Limongelli, M. P., Giordano, P. F. and Prendergast, L. J. Risk-based scour management: a
569 survey, In: *Bridge Maintenance, Safety, Management, Life-Cycle Sustainability and Innovations: Proceedings of the 10th*
570 *International Conference on Bridge Maintenance, Safety and Management (IABMAS 2020)*, Sapporo, Japan, 11-15 April
571 2021 (Yokota, H. & Frangopol, D.M. (eds.)). CRC Press/Balkema Taylor & Francis Group, The Netherlands, pp. 1258-
572 1264. <https://doi.org/10.1201/9780429279119-170>, 2021a.

573 Pregnolato, M., Winter, A.O., Mascarenas, D., Sen, A.D., Bates, P. and Motley, M.R.: An integrated impact analysis for
574 riverine bridges subjected to high river flows, In: *Bridge Maintenance, Safety, Management, Life-Cycle Sustainability and*
575 *Innovations: Proceedings of the 10th International Conference on Bridge Maintenance, Safety and Management (IABMAS*
576 *2020)*, Sapporo, Japan, 11-15 April 2021 (Yokota, H. & Frangopol, D.M. (eds.)). CRC Press/Balkema Taylor & Francis
577 Group, The Netherlands, pp. 693-701. <https://doi.org/10.1201/9780429279119-91>, 2021b.

578 Pregnolato, M.: Bridge safety is not for granted – A novel approach for bridge management, *Eng. Structures*, 196, 109193,
579 <https://doi.org/10.1016/j.engstruct.2019.05.035>, 2019.

580 Pregnolato M., Ford A., Robson C., Glenis V., Barr, S. and Dawson R.J.: Assessing Urban Strategies for Reducing the Impacts
581 of extreme Weather on Infrastructure Networks, *Royal Soc. Open Sci.*, 3(5), 1-15, doi: 10.1098/rsos.160023, 2016.

582 Qin, X., Motley, M.R. and Marafi, N.: Three-dimensional modeling of tsunami forces on coastal communities, *Coast. Eng.*,
583 140, 43–59, <https://doi.org/10.1016/j.coastaleng.2018.06.008>, 2018.

584 Solomon, S., Manning, M., Marquis, M. and Qin, D.: *Climate change 2007 - the physical science basis: Working group I*
585 *contribution to the 4th assessment report of the IPCC*, Cambridge University Press, Cambridge, 2007.

586 Stanton, J. F., Roeder, C. W., Mackenzie-Helnwein, P., White, C., Kuester, C., and Craig, B.: *Rotation Limits for Elastomeric*
587 *Bearings*, NCHRP Report 596, The National Academies Press, Washington D.C., doi: 10.17226/23131, 2008.

588 Stephens, M.T., Winter, A., Motley, M.R., and Lehman, D.E.: Comparing seismic and tsunami load demands on reinforced
589 concrete and concrete filled steel tube bridges, *Proceedings of the 39th IABSE Symposium*, 2017.

590 Tryggvason, G., Scardovelli, R. and Zaleski, S.: *Direct numerical simulations of gas–liquid multiphase flows*, Cambridge
591 University Press, Cambridge, 2011.

592 Yang, D. Y. and Frangopol, D.: Life-cycle management of deteriorating bridge networks with network-level risk bounds and
593 system reliability analysis, *Struct. Safety*, 83, 101911, <https://doi.org/10.1016/j.strusafe.2019.101911>, 2020.

594 Yilmaz, T., Banerjee, S. and Johnson, P. A.: Performance of two real-life California bridges under regional natural hazards. *J.*
595 *Bridge. Eng.* 21(3), 1–15, [https://doi.org/10.1061/\(ASCE\)BE.1943-5592.0000827](https://doi.org/10.1061/(ASCE)BE.1943-5592.0000827), 2016.

596 Yurday, E.: Average Cost to Run a Car UK 2020: <https://www.nimblefins.co.uk/average-cost-run-car-uk>, last access: 12 May
597 2020, 2020.

598 Wang, C., Yu, X. and Liang, F.: A review of bridge scour: mechanism, estimation, monitoring and countermeasures, Nat.
599 Hazards, 87, 1881–1906, <https://doi.org/10.1007/s11069-017-2842-2>, 2017.

600 Wardhana, K. and Hadipriono, F. C.: Analysis of Recent Bridge Failures in the United States, J. Perf. of Constructed Facilities
601 17(3), 144–150, [https://doi.org/10.1061/\(ASCE\)0887-3828\(2003\)17:3\(144\)](https://doi.org/10.1061/(ASCE)0887-3828(2003)17:3(144)), 2003.

602 Werner, S. D., Cho, S. and Eguchi, R. T.: The ShakeOut Scenario Supplemental Study: Analysis of Risks to Southern
603 California Highway System, SPA Risk LLC, Denver, CO, 2008.

604 Winter, A.O., Motley M.R. and Eberhard M.O.: Tsunami-like wave loading of individual bridge components, J. Bridge Eng.
605 23 (2), 04017137, [https://doi.org/10.1061/\(ASCE\)BE.1943-5592.0001177](https://doi.org/10.1061/(ASCE)BE.1943-5592.0001177), 2017.

606 Zhou, Y., Banerjee, S. and Shinozuka, M.: Socio-economic effect of seismic retrofit of bridges for highway transportation
607 networks: a pilot study, Struct. Infrastruct. Eng. 6, 145-157, <https://doi.org/10.1080/15732470802663862>, 2010